UNIVERSITY OF LEEDS

Article:
Bradley, D, Lawes, M orcid.org/0000-0002-8693-7536 and Morsy, ME (2019) Measurement of turbulence characteristics in a large scale fan-stirred spherical vessel. Journal of Turbulence, 20 (3). TJOT 1610566. pp. 195-213. ISSN 1468-5248

https://doi.org/10.1080/14685248.2019.1610566

Measurement of Turbulence Characteristics in a Large Scale Fan-Stirred Spherical Vessel

Derek Bradley*, Malcolm Lawes** & Mohamed Elsayed Morsy***

School of Mechanical Engineering, University of Leeds, Leeds LS2 9JT, UK

*Corresponding author: d.bradley@leeds.ac.uk

** Contact E-mail: m.lawes@leeds.ac.uk

*** Contact E-mail: me_nl@yahoo.com

Measurement of Turbulence Characteristics in a Large Scale Fan-Stirred Spherical Vessel

Particle Image Velocimetry, PIV, is employed to characterise the near-homogeneous, isotropic, turbulence generated inside a large spherical vessel by four rotating fans. Spatial and temporal distributions of mean and root mean square, rms, velocity fluctuations are investigated, as well as integral length scales, L, Taylor microscales, λ, and Kolmogorov length scales, η, in the fan speed range, 1,000-6,000 rpm. Mean velocities are about 10 % of the turbulence velocity, u' and turbulence is close to homogeneous and isotropic in the central volume. This volume decreases with increasing fan speed, and its radius and other characteristics are expressed in terms of the fan speed. At each speed, the mean gas velocity scarcely varies with time. Relationships are presented for the variations of u' and L with fan speed, temperature and pressure. A new relationship between the autocorrelation function and integral length scale is obtained, for when Taylor's hypothesis is invalid.

Keywords: Fan-Stirred Vessel; Turbulence; Homogeneous & isotropic flow; Length scales

1. Introduction

Not infrequently, it is convenient to suppress high convective velocities, in order to facilitate experimental studies of the influences of turbulence on such phenomena as phase changes, chemical reactions, generation of sprays, and flame propagation. A suitable vessel contains the turbulent liquid or gaseous mixture, with turbulence generated by one or more rotating fans. The detail that can be revealed in such a fan-stirred, probably spherical, vessel is also valuable, when considered in parallel with direct numerical simulations of the effects of such turbulence. Useful generalisation can be achieved for turbulence that is homogeneous and isotropic, and this has been widely discussed [1,2]. The mean flow should be minimal, with spatial and temporal uniformity of the rms turbulent velocity, u', and turbulent length scale, with near-Gaussian turbulent velocity

probability density functions, pdfs, all with good control, quantification, and repeatability.

The use of fans to control the turbulence, in a mixture initially at rest, was pioneered by Schlossing and de Mondesir in 1864, see [3]. Some stages in the sequential development of this technique are indicated in Table 1, along with details of the different vessels. Semenov [4] showed that four identical, eight-bladed fans, symmetrically disposed within a closed volume, rotating at the same speed, generated a central region of uniform isotropic turbulence. Sokolik et al. [9] employed this technique, in a vessel of about 97 mm radius and rms velocity of up to 10 m/s, with pressure records and flame photography, to measure turbulent burning velocities. Andrews et al. [3] employed a cylindrical explosion vessel, with fan speeds up to 5,000 rpm and rms turbulent velocities, u', up to 4 m/s. Hot wire anemometry confirmed a high degree of isotropy. Abdel-Gayed et al. [10], in measuring turbulent burning velocities, used laser Doppler velocimetry to measure u', and the turbulent length scales.

Hwang & Eaton [1] created an approximately spherical Plexiglas chamber, with homogeneous, isotropic turbulence, generated by eight synthetic jet actuators. Two-dimensional particle image velocimetry, PIV, measured turbulent rms velocities of 0.87 m/s, corresponding to a Taylor microscale Reynolds number, R_λ, of 218. Bradley et al. [11,12] showed the turbulent burning velocity and flame wrinkling rate to depend on turbulence statistics, such as u', and the turbulent length scales. The consistency of turbulent burning velocity measurements relies on the ability to attain near- isotropic and homogeneous turbulence, with well-defined turbulence statistics. More recently, Weiß et al. [7] have employed a stainless steel cuboid vessel of 22.28 litres capacity, with eight variable speed fans. Turbulence characteristics were measured by both laser Doppler velocimetry, LDV, and PIV. Values of u' measured by PIV were up to 30% smaller than

those measured by LDV. Ravi et al. [2] employed four impellers, with different geometries, in a cylindrical vessel and measured rms turbulent velocities between 1.2 and 1.7 m/s, using PIV. The high repetition PIV measurement technique yields more reliable temporal and spatial data. Xu et al. [8] employed a cubic explosion vessel, with two opposed four bladed fans, giving maximum u' values of 1.6 m/s at 2,900 rpm. Characteristics were measured with PIV, and three sheet velocity fields were measured to reconstruct the 3D boundary of the homogenous region.

In the case of combustion studies of spherical explosions, the vessel and windows must be large enough for a stable flame to be established and observed at near constant pressure. Also, ideally, the subsequent onset of flame instability as the stretch rate decreases, should be observable. Table 1 shows the current vessel to be relatively large, with large u'.

The present paper provides background data for the design of such vessel, and also reports the detailed use of high repetition rate PIV to generate information about the turbulent velocity maps in the vessel and assess the turbulence data, for dry air in the absence of phase change and chemical reaction. First, spatial and temporal fluctuations of the mean velocities and rms velocities are presented at different fan speeds, in the range 1,000-6,000 rpm. The mean velocity within each interrogation area is shown to be almost negligible compared with u'. After describing the experimental approach adopted, the sequential detailed coverage is:

(i). Determination of the extent of the central homogenous volume of isotropic turbulence at different fan speeds.

(ii). Derivation of the probability density function of velocity fluctuations normalised by the local rms value.

(iii). Measurement of turbulent length scales as a function of fan speed.

(iv). Effects of pressure and temperature changes of the air on rms velocities and turbulent length scales at different fan speeds. A relationship is developed between the autocorrelation function and integral length scale and presented, for conditions when Taylor's hypothesis is invalid.

2. The fan-stirred vessel

The measurements were made in a spherical stainless steel explosion vessel with an inner diameter of 380 mm. The vessel has three pairs of optical flat and non-conformal quartz windows of 150 mm diameter, allowing a full visualisation of the centre of the chamber. Four identical fans, each powered by an 8 kW three phase electric motor, are located close to the wall of the vessel. These are arranged in a regular tetrahedron configuration, in an attempt to optimise homogenous, isotropic turbulence, as shown in Figures 1 and 2. Each fan has 8 blades, of about 75 mm length, and these are about 72 mm apart at their edges. They were controlled by individual solid state variable frequency convertors, with a speed control range of 200-10,000 rpm (3.3-176 Hz), in increments of 20-30 rpm. [Figures 1 and 2 near here]

Two pressure transducers were mounted flush with the inner surface of the vessel wall, one for static, and the other for dynamic measurements in explosion studies. Only the static transducer was used, to study the effect of pressure on the turbulence characteristics. The vessel could be heated by an internal 2 kW coiled heating element, attached to the inside of the access cover. The temperature was set, controlled, and displayed by a PID controller, (CAL Controls, CAL3200) mounted in the control panel, using feedback via a K-type thermocouple (25μm chromel-alumel wire). At a fan speed of 10,000 rpm, the dissipation of energy increased the temperature of the air at 0.1 MPa by 3 K.

A high repetition rate double pulsed Nd:YAG laser (DM60-DH, Photonics), is employed to generate pulses of 12 mJ at a wavelength of 532 nm at 5 KHz. The laser beam is expanded into a vertical sheet of about 0.5 mm thickness, in passing through the centre of the vessel, where it uniformly illuminates the dispersed seeding particles of olive oil, < 1 μm diameter, generated by six jet atomisers (9010F0021, DANTEC). The measuring system comprises a spherical lens of 300 mm and a cylindrical lens of -25 mm focal length. The laser pulses, were synchronized with a high-speed camera perpendicular to the laser sheet, to record a 12-bit image pair of 1024×1024 pixels. The time between pulses was varied from 15 to 35 μs, depending on the fan speed. With this configuration, it was possible to measure the instantaneous velocities of the flow within a radius of 60 mm, from the vessel centre. Each experiment was undertaken during about 2.5s, with the collection of an average of 12,500 images. An adaptive algorithm within the Dantec software, processed the images, with a minimum interrogation area of (16×16 pixels) and a maximum of (32×32 pixels), with a magnification ratio of 0.12 mm/pixel. This adaptive PIV algorithm was an iterative and automatic way of calculating velocity vectors, based on the seeding particle density. The size and shape of individual interrogation areas, IA, were iteratively adjusted to fit the local seeding densities and velocity gradients. The appropriate IA size was automatically determined for each individual IA, by specifying maximum and minimum size limits. A first iteration always used the largest IA size, which was reduced in subsequent iterations. This allowed reduction of IA sizes where the particle density was sufficiently high. The minimum IA determined the location and magnitude of vectors, and how close to the borders a vector might be located. Further details about the PIV system, its optical configuration and the adaptive algorithm are to be found in [13] and in the supplementary material [S1].

3. Homogeneity and isotropy

3.1. Instantaneous, mean and rms velocities

The mean velocities and rms turbulent velocity fluctuations in the x- and y-directions, respectively, noted $\bar{u}$, $\bar{v}$, u' and v', are determined from the temporal evolution of the instantaneous velocities u and v, respectively. In the x-direction, $\bar{u}$ and u' are calculated at each (x, y) grid node as [14]:

$$\bar{u}(x,y) = \frac{1}{N_{im}} \sum_{i=1}^{N_{im}} u(x,y,i). \quad (1)$$

and

$$u'(x,y) = \sqrt{\frac{1}{N_{im}} \sum_{i=1}^{N_{im}} [u(x,y,i) - \bar{u}(x,y)]^2}. \quad (2)$$

Where N_{im} is the total number of vectors, in the i_{th} vector map in time. The crossponding parameters in the y-direction, $\bar{v}$ and v', are calculated in the same way, by replacing u and $\bar{u}$, in equations (1) and (2), by v and $\bar{v}$, respectively. The ways in which the instantaneous and mean velocities change with increasing fan speeds of 1,000, 3,000, and 6,000 rpm are shown in Figure 3. For clarity, only half the vectors are displayed. The first column shows instantaneous velocities at all points, with colouring to show the magnitude of the two component velocity vectors. The second column shows time averaged local mean velocity vectors obtained, from 12,500 images. Both instantaneous and mean velocities increase with fan speed and radius, most markedly in the outer regions closest to the fans. Within the centralised circled regions in Figure 3b, the local mean velocity is less than 10% of the local rms velocity. Outside the circles mean velocities reach up to $\pm$0.4, $\pm$1.2 and $\pm$1.4 m/s at 1,000, 3,000 and 6,000 rpm, respectively. However, there is a similarity in flow patterns at all fan speeds, and the mean velocities are generally low.

[Figure 3 near here]

Figure 4 shows the radial distributions of mean velocities, $\bar{u}_x$, $\bar{u}_y$, $\bar{v}_x$ and $\bar{v}_y$ for fan speeds of 1,000 and 6,000 rpm. Data were obtained from 12,500 frames during a time of 2.5 s .The velocity components $\bar{u}_x$ and $\bar{v}_x$ were calculated along the x- axis for $y = 0$. Whilst, $\bar{u}_y$ and $\bar{v}_y$, were calculated along the y-axis for $x = 0$. The variations of the four components are small and their fluctuations are almost uniform, for x and y distances of $\pm$ 60 mm, indicative of a high level of isotropy. At the higher fan speed of 6,000 rpm, slight increases and decreases in velocities, of less than 0.95 m/s, are observed beyond a radius of $\pm$ 40 mm. Nevertheless, the values of the four components are small when compared with those of u' and v'. [Figure 4 near here]

Figure 5 compares the spatial fluctuations of both mean and rms velocities, $\bar{u}$, $\bar{v}$, u' and v' along x- and y-axes at fan speeds of 1,000, 3,000 and 6,000 rpm. For both mean and rms velocities, x and y components are similar and isotropic, with $\bar{u}$ and $\bar{v}$ small and less than $0.1u'$. Isotropy and homogeneity are particularly good in the central region at radii up to about 50 mm. However, closer to the fans, at the higher speed of 6,000 rpm and radii greater than 40 mm, isotropy and homogeneity are less good. Average values of $\bar{u}$, $\bar{v}$, u' and v' were computed up to a radius of 60 mm for all fan speeds and these are summarised in Table 2. [Figure 5 and Table 2 near here]

All measurements geometrically involved the same plane, passing through the centre of the vessel, and the tetrahedral positioning of the fans was intended to maximise the isotropy and homogeneity over other orthogonal planes. According to [1-2, 5, 8], an area can be considered to be homogeneous area if ($\bar{u} < 10\%\, u'$ and $\bar{v} < 10\%\, v'$). Such parameters have been calculated at each interrogation area and the crossponding area which satisfy these condition has been assigned. The radial limit, within which there is homogeneity and isotropy is R_H and this is shown, for different fan speeds in Figure 6. Values of u' were estimated for each interrogation window and then averaged over all the interrogation

windows within the area of interest. These values also are plotted on the same figure. A linear fit applied to these measurements yields:

$$u' = 0.00122f(rpm) \quad (m/s). \tag{3}$$

These values are up to 5% higher than earlier single point measurements using laser Doppler velocimetry, LDV. This slight difference might be because of the difference in technique, and because the PIV data were averaged over a larger area, with a diameter of 120 mm, whereas the LDV data in [15] were obtained only at the vessel centre. [Figure 6 near here]

3.2. Pdfs of turbulent velocity

Turbulent velocity fluctuations u_N and v_N about the mean, normalised by the local rms value, are calculated as in [16]. u_N is given by:

$$u_N(x, y, i) = [u(x, y, i) - \bar{u}(x, y)]/u'(x, y). \tag{4}$$

v_N can be calculated using equation (4), by replacing u, $\bar{u}$ and u' by v, $\bar{v}$ and v', respectively. Figure 7 shows the pdfs of u_N and v_N for fan speeds of 1,000 rpm and 6,000 rpm. The results of all pdfs appear to be consistent with normal Gaussian distributions. To more precisely quantify the symmetry of the pdfs, and whether the data are heavy-tailed or light-tailed relative to a normal distribution, the skewness factor, S_k, and kurtosis factor, K, were evaluated. In x-direction, S_k and K are given by [14]:

$$S_{k,u} = \frac{1}{n}\sum_{j=1}^{n}\left(\frac{\frac{1}{N_{im}}\sqrt{\sum_{i=1}^{N_{im}}[u(x, y, i) - \bar{u}(x, y)]^3}}{[u'(x, y)]^3}\right). \tag{5}$$

and,

$$K_u = \frac{1}{n}\sum_{j=1}^{n}\left(\frac{\frac{1}{N_{im}}\sqrt{\sum_{i=1}^{N_{im}}[u(x,y,i)-\bar{u}(x,y)]^4}}{[u'(x,y)]^4}\right). \quad (6)$$

Here n is the total number of grid nodes in the vector map. The crossponding skewness and kurtosis in the y-direction respectively, noted $S_{k,v}$ and K_v, are calculated in the same way, by using v, $\bar{v}$ and v', in equations (5) and (6), instead of u, $\bar{u}$ and u', respectivly. Figure 8 shows the variations of S_u, S_v, K_u and K_v with fan speed. The skewness factors S_u and S_v are close to zero, indicating a symmetric pdf. Also, the kurtosis factors, K_u and K_v, are close to the kurtosis factor, $K = 3$, of a normal Gaussian curve. These results supports the assumption in [10] for calculating the integral length scale, that the kurtosis and skewness factors are independent of the fan speed. The results of Sections 3.1 and 3.2 confirm these features of homogenous and isotropic flow, within the defined regions. [Figure 7 and 8 near here]

4. Turbulence scales

4.1. Integral length scales

The spatial longitudinal and lateral integral lengths scales L_{ux}, L_{vy} and L_{uy}, L_{vx}, can be determined directly from the integral of the correlation coefficients, R_{ux}, R_{vy} and R_{uy}, R_{vx}, respectively, of the fluctuating velocity values in x-direction and in y-diraction [16]. In x-direction, R_{ux} and R_{vx} are calculated as [14]:

$$R_{ux}(\xi) = \frac{\langle u(x,y)u(x+\xi,y)\rangle}{u'^2}, \quad L_{ux} = \int_0^{R_0} R_{ux}(\xi)\, d\xi. \quad (7)$$

$$R_{vx}(\xi) = \frac{\langle v(x,y)v(x+\xi,y)\rangle}{v'^2}, \quad L_{vx} = \int_0^{R_0} R_{vx}(\xi)\, d\xi. \quad (8)$$

Equations (7) and (8) are employed to calculate R_{uy} and R_{vy}, in y-direction [14]. A sufficiently large area, 90×90 mm^2, was used to calculate the integral length scales. For all fan speeds, this area was large enough for the correlation coefficient to become zero,

R_o [2,17]. Figure 9 shows such an evolution of the longitudinal and lateral correlation coefficients with the spatial lag at a fan speed of 5,000 rpm. The very slight differences between the two longitudinal correlation coefficients R_{ux} and R_{vy} and similar to the differences between the lateral coefficients R_{uy} and R_{vx}, confirming the near isotropic nature of the flow field within the central area. [Figure 9 near here]

Figure 10 shows the variations of longitudinal and lateral integral length scales, L_{ux}, L_{vy} and L_{uy}, L_{vx} with fan speed, giving mean longitudinal and lateral length scales of 20.4 and 10.5 mm, respectively. Such independence of fan speed has been commonly observed [18,19]. [Figure 10 near here]

4.2. Taylor and Kolmogorov scales

According to [18,19], the Taylor length scale, λ, is related to the turbulence dissipation rate, ε, by:

$$\lambda = (15\nu\langle u^2\rangle/\langle\varepsilon\rangle)^2 \tag{9}$$

where ν is the kinematic viscosity, values of which were obtained from [20] and $\langle\,\rangle$ denotes time averaging. The crossponding Reynolds number is given by, $R_\lambda = \lambda u'/\nu$ [18]. For homogeneous and isotropic flow, the turbulent energy dissipation rate, ε, is defined by [21] as:

$$\varepsilon = 15\nu\left\langle\left(\frac{\partial u}{\partial x}\right)^2\right\rangle \tag{10}$$

The dissipation rate can be calculated directly from the PIV vector maps by using the velocity spatial derivatives in equation (10). To account for the error of the finite spatial resolution of PIV measurements, a correction method to the dissipation rate, ε, have been proposed by [22]. The correction includes filtering a known energy spectrum to account for the attenuation of the derivatives in the measured PIV data. The ratio of the measured

derivative, denoted by the superscript (m), to the ‘‘corrected’’ derivative for the longitudinal measurement is given by [22] as:

$$\frac{\varepsilon^m}{\varepsilon} = \frac{\langle(\partial u_x/\partial x_x)^2\rangle^m}{\langle(\partial u_x/\partial x_x)^2\rangle} = \frac{\iiint_{-\infty}^{\infty} B^2 \frac{\sin^2(\Delta x_x k_x/2)}{(\Delta x_x/2)^2} \Phi_{xx}(\underline{k}) dk_x dk_y dk_z}{\iiint_{-\infty}^{\infty} k_x^2 \Phi_{xx}(\underline{k}) dk_x dk_y dk_z} \quad (11)$$

where B is the spatial spectral filtering function given by:

$$B = \frac{8}{(wk_x)(hk_y)(zk_z)} sin\left(\frac{k_x w}{2}\right) sin\left(\frac{k_y h}{2}\right) sin\left(\frac{k_z z}{2}\right) \quad (12)$$

and,

$$\Phi_{xx}(\underline{k}) = \frac{E(k)}{4\pi k^{-4}} (k^2 \delta_{xx} - k_x k_x) \quad (13)$$

where $\underline{k}$ is the wavenumber vector with a magnitude k and $k_x, k_y$and k_z are the wave vector components in the x, y and z directions. The variable $w, h, s, \Delta x_x$ correspond to the width, height, and depth of the PIV interrogation volume and the separation between PIV vectors respectively. $E(k)$ is the 3D energy spectrum, which is defined by [23] as:

$$E(k) = \alpha u_\eta^2 \eta\left((k\eta)^{-5/3} + (k\eta)^1\right) \times \exp\left[-\alpha\left(\frac{3}{2}(k\eta)^{4/3} + (k\eta)^2\right)\right] \quad (14)$$

With α = 1.8, u_η is the Kolmogorov velocity scale, $= (\nu\varepsilon)^{1/4}$, and η is the Kolmogorov length scale given by [18]:

$$\eta = (\nu^3/\varepsilon)^{1/4} \quad (15)$$

An alternative correction method to the dissipation rate, based on the average distance between consecutive zero- crossings of $u(x)$, can be found in [24]. To calculate Taylor and Kolmogorov length scales, the corrected dissipation rate, ε, was first computed using equations (10) to (14) and then substituted into equations (9) and (15), respectively. As shown in Figure 10, λ and η decrease with increasing fan speed. Since L is fixed by the vessel dimensions, increasing Reynolds number $R_L, = Lu'/\nu$ [25], with the fan speed increases the dissipation rate and leads to finer length scales. Values of the different mean

length scales, up to a radius of 60 mm, are tabulated in Table 3 for the fan speed range 1,000 to 6,000 rpm, for dry atmospheric air temperatures and pressures. In practice, integral length scales are predominantly determined by the vessel size. In the present case, the diameter of 380 mm is about 19 times larger than L_{ux}, L_{vy}. Clearly, this will be modified by the locations and sizes of the fans and their blades. [Figure 10 and Table 3 near here]

The one-dimension temporal energy spectra, E_{ux} and E_{vy}, of the velocity fluctuations u and v were computed, using a procedure similar to that outlined in [26]. They were first computed for each interrogation area, IA, and then averaged over all the IAs, within the velocity map. Figure 11 shows average values of energy spectra, E, of the two components E_{Ux} and E_{Vy}, for three rotational speeds of 1,000, 3,000 and 6,000 rpm. The corresponding Reynolds numbers, R_L, are reported in Table 3. This figure highlights the inertial subrange, characterised by a (-5/3) scaling law exponent, is extending with R_L, as predicated by the Kolmogorov theory. [Figure 11 near here]

4.3. Integral time scale

At a given point, integral time scales, τ_u and $\tau_{v,}$ are calculated by the integration of the temporal coefficients R_u and R_v [13]. R_u is given by:

$$R_u(t) = \frac{u(t)u(t+\Delta t)}{u'^2}\ ,\ \tau_u = \int_0^{R_0} R_u(t)\ dt. \qquad (16)$$

R_v can be calculated from equation (16) by using v and v' instead of u and u', respectively. These coefficients are plotted in Figure 12, for a fan speed of 1,000 rpm. They are calculated for each interrogation area and then averaged overall interrogation areas within the velocity map. They are closely matched, again indicative of isotropy. The integral length scale L is usually related to the integral timescale τ by Taylor's temporal hypothesis: $L = \bar{u}\tau$, where $\bar{u}$, here, is the advection mean velocity. This is clearly

inapplicable when $\bar{u}$ is close to zero, as in the current case. To overcome this, Abdel-Gayed et al. [10] employed $L = \bar{S}\tau$, with $\bar{S}$, the average speed with a three-dimensional Gaussian velocity pdf in isotropic, homogeneous turbulence, given by $\bar{S} = (8/\pi)^{0.5}\, u'$. Hence L could be found from:

$$L = (8/\pi)^{0.5} u'\, \tau. \tag{17}$$

[Figure 12 near here]

Advances in measuring techniques have enabled both L and τ to be measured directly, and the validity of equation (17) to be assessed. Both L/τ and τ are plotted against u' in Figure 13. Five experiments were employed for each condition. A linear fit to the data yielded $L = 0.88\, u'\tau$. Figure 14 shows the mean longitudinal correlation coefficient $R(\xi)$ as a function of the spatial shift (ξ), the mean temporal correlation coefficient $R(L/\tau.t)$ as a function of the product of PIV values of $(L/\tau.t)$ and the mean temporal correlation coefficient $R(\bar{s}.t)$ as a function of the product of $(\bar{s}.t)$, where $\bar{s}$ is the average speed, with a three-dimensional Gaussian velocity pdf in isotropic, homogeneous turbulence as defined by [10]. Such figure shows $R(\bar{s}.t)$ does not coincide with $R(\xi)$, which suggests that the proportionality constant of 0.88, is more acceptable, compared to 1.6 in equation (17). This result is of practical importance, because optical access often is limited to single point LDV. [Figure 13 and 14 near here]

5. Influence of temperature and pressure

Shown, by solid curves, in Figure 15 are the effects of temperature on the temporal rms velocities u' and v' at fan speeds of 1,000, 3,000 and 6,000 rpm at 0.1 MPa. Regardless of the increasing temperature, the values of both u' and v' are very close, at the different fan speeds, suggesting the maintenance of a homogenous isotropic structure of the flow. At fan speeds of 1,000 and 3,000 rpm, there is only a small effect of temperature on the

values of u' and v'. At a fan speed 6,000 rpm, the increase in temperature decreases values of u' and v' by up to 12% of the value at 300 K. This might be associated with increases in kinematic viscosity with increasing T. [Figure 15 near here]

In the same figure, Fig. 15, the effect of pressure on the temporal rms velocities u' and v' at fan speeds 1,000, 3,000 and 6,000 rpm at 300 K is shown by broken curves. Increasing pressure showed even smaller changes in the values u' and v' with increasing P, which, in this case, slightly increased. The largest effect was at the highest fan speed, possibly associated with a small decrease in kinematic viscosity with increasing P.

The effects of increasing temperatures and pressures on the integral length scale, and the smaller Taylor and Komogorov scales are shown in Figures 16 and 17, all for a fan speed of 1,000 rpm. Figure 16 shows the effect of temperature on length scales at a pressure of 0.1 MPa. This shows the integral length scale, L, Taylor length scale, λ, and Kolmogorov length scale, η, are increased by up to 10 %, 47 % and 36.5%, respectively, of their values at 300 K. Such increases can be related to the increase in the kinematic viscosity with temperature in equations (9) and (15). Figure 17 shows the effect of pressure on L, λ, and η at 300 K. Increasing the pressure has no effect on the integral length scales, it generates smaller eddies and consequently smaller lengths scales. Both values of λ and η decrease, with increasing the pressure, which agrees with the trend in [5]. As shown in [27], for isotropic and homogenous flow, the Taylor length scale varies as $P^{-1/2}$, and the Kolmogorov varies as $P^{-3/4}$. These trends have been observed in the present results at different fan speed. These results are summarised in the supplementary material [S2], Tables S1 and S2, for different temperatures and pressures. [Figure 16 and 17 near here]

6. Conclusions

(1). Spatial and temporal fluctuations of mean and rms velocities have been presented at different fan speeds between 1,000 and 6,000 rpm. The mean velocity within each interrogation area has been shown to be negligible, compared with the rms turbulent velocity.

(2). The region of homogeneity and isotropy decreases with increasing fan speed. The maximum radius, R_H, of this region is given in terms of the fan speed and u' in Figure 6.

(3). Probability density functions have been derived for the turbulent velocity fluctuations about the mean, and normalised by the localised rms values. Within the isotropic region these are very close to a Gaussian distribution, for both velocities.

(4). The size of the isotropic region is an important design parameter, as it must be large enough to be able to generate all the required phenomena at near-constant pressure, and the size of the window must be large enough to observe it. The study provides a guide to the design of, and characteristics of, fan-stirred bombs, and also the extent to which the turbulence in the working volume is homogeneous and isotropic.

(5). Longitudinal and lateral integral length scales of the turbulence were obtained by integration of the respective correlation coefficients. Values of the length scales L_{ux} and L_{vy} are similar, as are those of L_{uy} and L_{vx}. These differ for the two sets, but are independent of the fan speed. Taylor and Kolmogorov length scales, obtained from algebraic expressions, are also presented.

(6). Similarly, integral time scale values, τ, have been found from integration of the respective temporal coefficients. These are equal for both directions. The length and temporal integral scales are related by $L = 0.88\, u'\tau$, somewhat more direct than an earlier expression.

(7). At low fan speeds and 0.1 MPa, there is little effect of temperature upon u' and v', whereas, at f = 6,000 rpm these values decrease with increasing temperature. At low fan speeds and 300 K, there is but small effect of pressure change, but at 6,000 rpm there is a slight increase in velocities with increasing pressures. With regard to the integral length scales, at 1,000 rpm, the integral length scales are unchanged with pressure, but increase slightly with temperature.

Funding

This publication is based on work supported by the British Council, the University of Helwan and the Egyptian Cultural Educational Bureau in London.

References

[1] Hwang W, Eaton JK .Creating homogeneous and isotropic turbulence without a mean flow. Exp Fluids. 2004;36:444–454.

[2] Ravi S, Peltier SJ, Petersen EL. Analysis of the impact of impeller geometry on the turbulent statistics inside a fan-stirred, cylindrical flame speed vessel using PIV. Exp Fluids. 2013;54 (1):1424.

[3] Andrews GE, Bradley D, Lwakabamba SB. Measurement of turbulent burning velocity for large turbulent Reynolds numbers. Int Symp Combust. 1975;15: 655-664.

[4] Semenov ES. Measurement of turbulence characteristics in a closed volume with artificial turbulence. Combust Explos Shock Waves. 1965;1(2):57-62.

[5] Fansler TD, Groff EG. Turbulence characteristics of a fan-stirred combustion vessel. Combust Flame. 1990; 80(3-4):350-354.

[6] Sick V, Hartman MR, Arpaci VS, et al. Turbulent scales in a fan-stirred combustion bomb. Combust Flame. 2001;127 (3):2119-2123.

[7] Weiß M, Zarzalis N, Suntz R. Experimental study of Markstein number effects on laminar flamelet velocity in turbulent premixed flames. Combust Flame. 2008;154 (4):671-691.

[8] Xu S, Huang S, Huang R, et al. Estimation of turbulence characteristics from PIV in a high-pressure fan-stirred constant volume combustion chamber. Appl Therm Eng. 2017;110:346-355.

[9] Sokolik AS, Karpov VP, Semenov ES. Turbulent combustion of gases. Combust Explos Shock Waves. 1967;3 (1):36-45.

[10] Abdel-Gayed RG, Al-Khishali KJ & Bradley D. Turbulent burning velocities and flame straining in explosions. Proc R Soc Lond A. 1984; 391(1801): 393-414.

[11] Bradley, D., Haq, M. Z., Hicks, R. A., Kitagawa, T., Lawes, M., Sheppard, C. G. W., & Woolley, R.. Turbulent burning velocity, burned gas distribution, and associated flame surface definition. Combust Flame. 2003;133(4):415-430.

[12] Bradley D, Lau AKC, Lawes M. Flame stretch rate as a determinant of turbulent burning velocity. Phil Trans R Soc Lond A. 1992;338 (1650):359-387.

[13] Bradley D, Lawes M, Morsy ME. Flame speed and particle image velocimetry measurements of laminar burning velocities and Markstein numbers of some hydrocarbons. Fuel, 2019; (243): 423-432.

[14] Goulier J, Chaumeix N, Halter F, et al. Experimental study of laminar and turbulent flame speed of a spherical flame in a fan-stirred closed vessel for hydrogen safety application. Nucl Eng Des. 2017; 312:214-227.

[15] Bradley D, Sheppard CGW, Suardjaja IM, et al. Fundamentals of high-energy spark ignition with lasers. Combust Flame 2004;138 (1-2): 55-77.

[16] Galmiche B, Mazellier N, Halter F, et al. Turbulence characterization of a high-pressure high-temperature fan-stirred combustion vessel using LDV, PIV and TR-PIV measurements. Exp Fluids. 2014; 55 (1):1636.

[17] De Jong J, Cao L, Woodward SH, et al. Dissipation rate estimation from PIV in zero-mean isotropic turbulence. Exp Fluids. 2009;46(3):499.

[18] McComb WD. The Physics of Fluid Turbulence. Oxford University Press.1990.

[19] Pasquier N, Lecordier B, Trinite M, et al. An experimental investigation of flame propagation through a turbulent stratified mixture. Proc Combust Inst. 2007; 31 (1):1567-1574.

[20] Morley C. Gaseq: a chemical equilibrium program for Windows. Ver. 0.79. 2005.

[21] Hinze JO. Turbulence McGraw-Hill. New York. 1975; 218:457.

[22] Lavoie P, Avallone G, De Gregorio F, et al. Spatial resolution of PIV for the measurement of turbulence. Exp Fluids. 2007; 43(1): 39-51.

[23] Lin JT. Velocity spectrum of locally isotropic turbulence in the inertial and dissipation ranges. The Physics of Fluids. 1972;15(1): 205-7.

[24] Fragner R, Mazellier N, Halter F, et al. Multi-scale high intensity turbulence generator applied to a high pressure turbulent burner. Flow Turbul. Combust. 2015; 94(1):263-83.

[25] Tennekes H, Lumley JL. A first course in turbulence. MIT press; 1972.

[26] Doron P, Bertuccioli L, Katz J, et al. Turbulence characteristics and dissipation estimates in the coastal ocean bottom boundary layer from PIV data. J Phys Oceanogr. 2001; 31(8): 2108-34.

[27] Lachaux T, Halter F, Chauveau C, et al. Flame front analysis of high-pressure turbulent lean premixed methane–air flames. Proc. Combust. Inst. 2005;30(1):819-82.

Table 1. Survey of some fan-stirred vessels, including present study.

	Vessel Geometry	Dimensions (mm)	Number of fans	Max. fan speed (rpm)	Max. u' (m/s)
Ravi et al. [2]	Cylindrical	D = 305, l = 356	4	8,300	1.7
Andrews et al.[3]	Cylindrical	D = 305, l = 305	4	5,000	4
Semenov [4]	Spherical	D = 97	4	7,000	10
Fansler et al.[5]	Cylindrical	D = 260, l = 260	4	2,500	2.2
Sick et al. [6]	Spherical	D = 58	4	7,000	1.8
Weiß et al. [7]	Spherical	D = 118	4	10,000	3.5
Xu et al. [8]	Cubic	l = 136	2	2,900	1.6
Present study	Spherical	D = 380	4	10,000	12

Table 2. Mean, rms velocities, skewness and kurtosis factors for all fan speeds.

Fan speed (rpm)	1,000	2,000	3,000	4,000	5,000	6,000
$\bar{u}$ (m/s)	0.04 ±0.02	0.22 ±0.04	0.14 ±0.02	0.25 ±0.04	0.51 ±0.04	0.71 ±0.04
$\bar{v}$ (m/s)	0.08 ±0.01	0.17 ±0.02	0.34 ±0.05	0.27 ±0.02	0.63 ±0.03	0.60 ±0.03
u' (m/s)	1.18 ±0.02	2.43 ±0.03	3.62 ±0.03	4.84 ±0.02	6.08 ±0.03	7.23 ±0.05
v' (m/s)	1.22 ±0.02	2.37 ±0.02	3.65 ±0.03	4.81 ±0.03	5.98 ±0.04	7.18 ±0.04
$S_{k,u}$	0.104	0.132	0.105	-0.212	0.282	-0.355
$S_{k,v}$	0.142	0.110	0.151	-0.264	0.232	-0.339
K_u	2.95	2.94	3.01	2.98	2.91	2.86
K_v	2.97	2.96	3.02	3.17	3.12	3.22

Table 3. Average values of the lengths scales for all fan speeds, at atmospheric temperature and pressure.

Fan speed (rpm)	R_L	R_λ	L_{ux} (mm)	L_{vy} (mm)	L_{uy} (mm)	L_{vx} (mm)	λ (mm)	$\eta \times 5$ (mm)
1,000	1,615	220.2	19.7	19.1	9.4	9.1	2.01	0.88
2,000	3,360	317.4	20.7	20.1	10.8	10.6	1.08	0.51
3,000	4,943	385.0	19.9	20.8	10.2	10.7	0.73	0.38
4,000	6,300	434.9	19.1	20.1	10.6	11.1	0.53	0.30
5,000	7,956	488.7	19.2	20.1	10.1	10.5	0.44	0.26
6,000	10,274	555.4	20.8	21.5	9.8	10.1	0.38	0.23

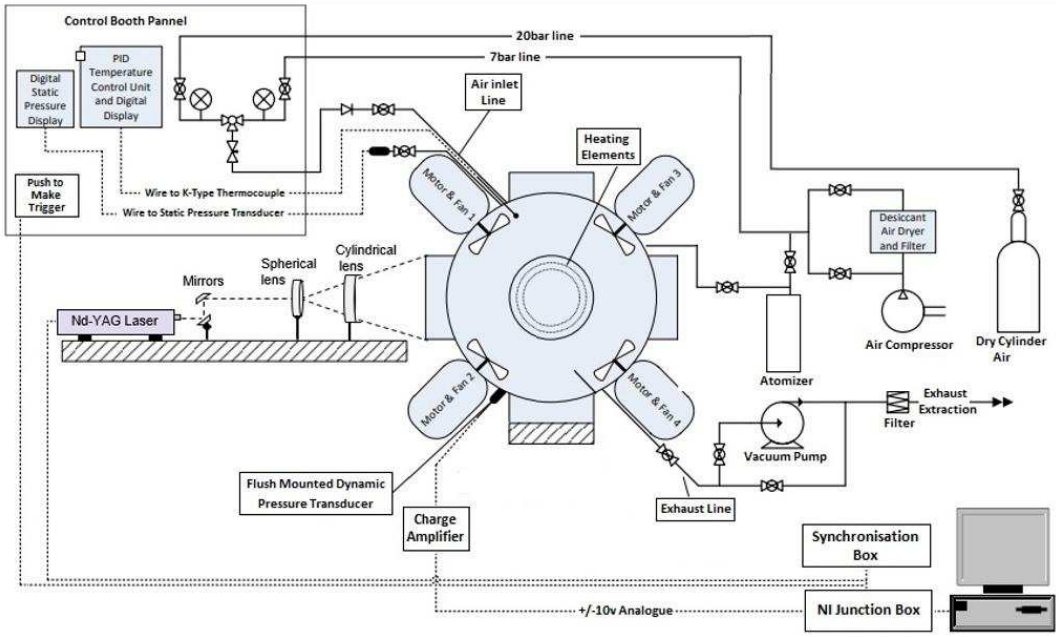

Figure 1. Schematic view of the vessel and auxiliary systems.

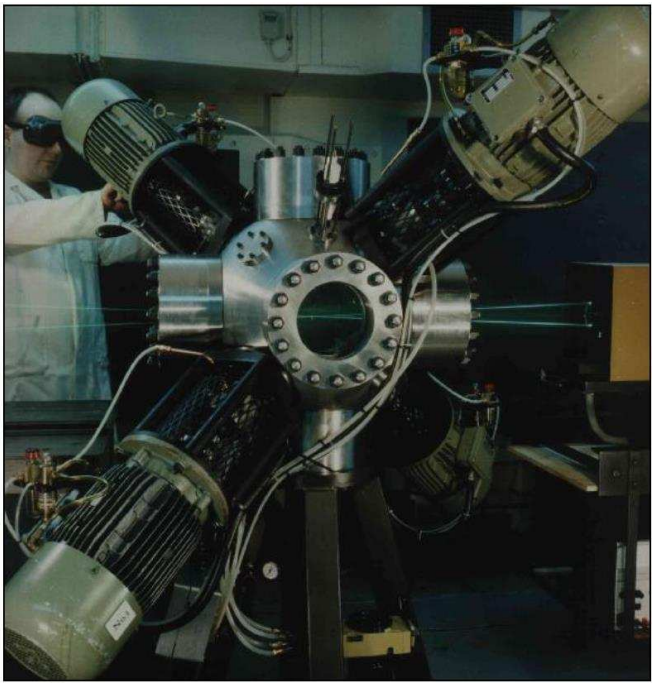

Figure 2. External view of the vessel

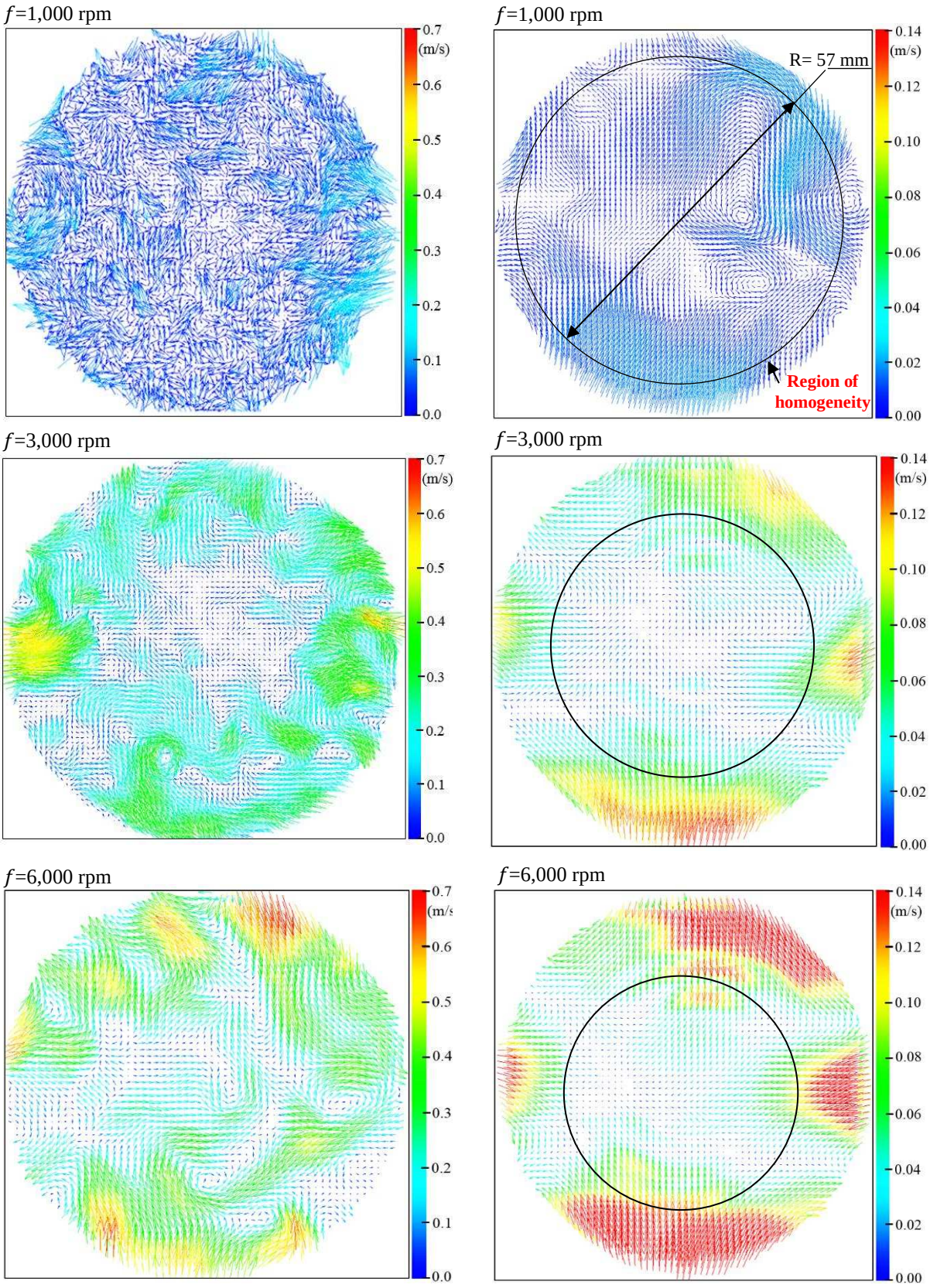

(a) Instantaneous velocity field. (b) Mean velocity field.

Figure 3. Examples of 2D velocity fields for fan speeds of 1,000, 3,000 and 6,000 rpm; scale (1:10); black circles show the region of homogeneity.

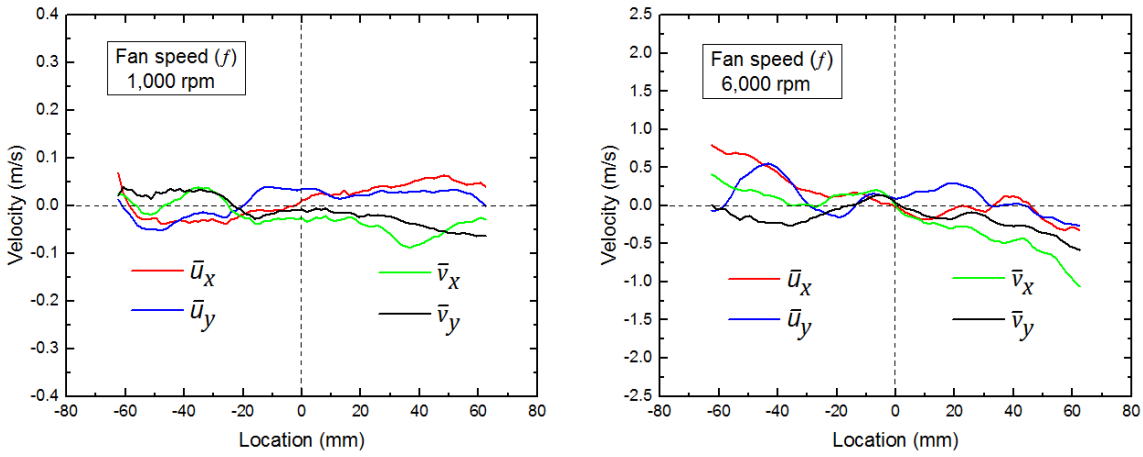

Figure 4. Spatial variations of mean velocities of $\bar{u}_x$, $\bar{u}_y$, $\bar{v}_x$ and $\bar{v}_y$ along x- and y-axes at fan speeds of 1,000 rpm and 6,000 rpm.

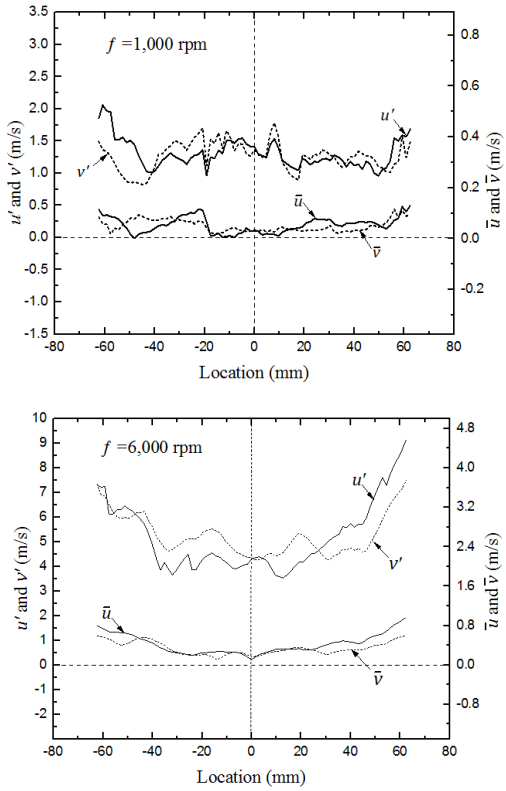

Figure 5. Spatial variations of $\bar{u}$ and u' along x-axis and of $\bar{v}$ and v' along y-axis, at fan speeds of 1,000, 3,000 and 6,000 rpm.

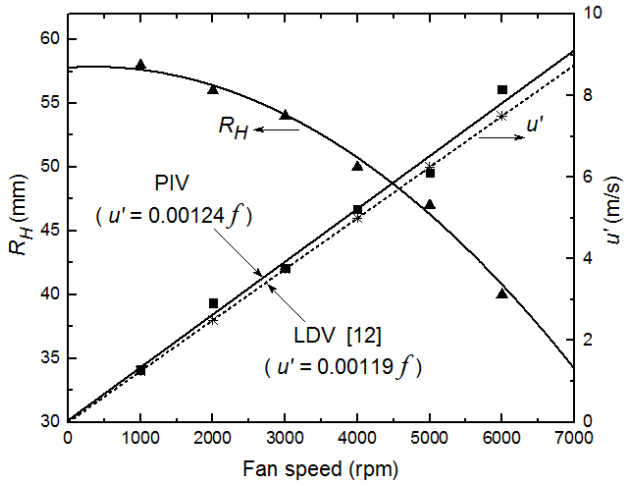

Figure 6. Effect of fan speed on the radial extent of homogenous, isotropic turbulence.

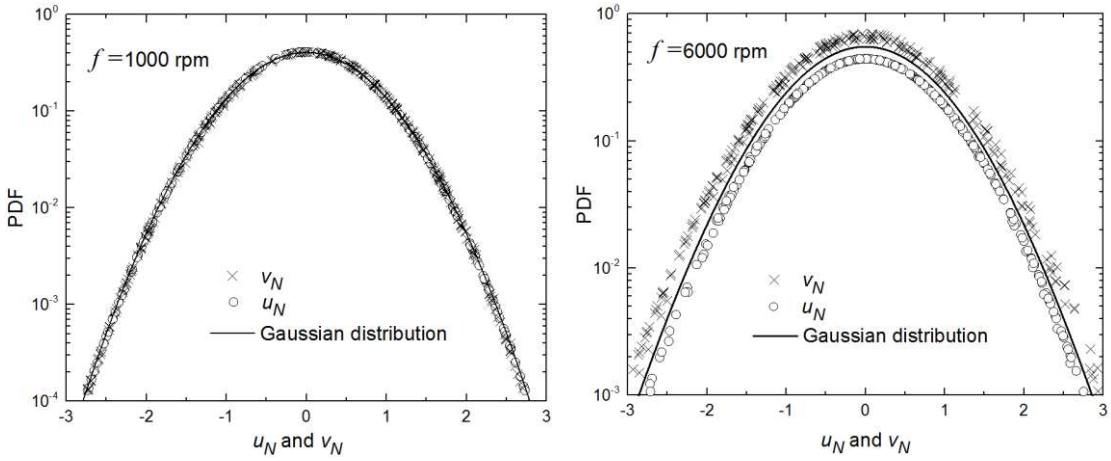

Figure 7. Pdfs of u_N and v_N at different fan speeds

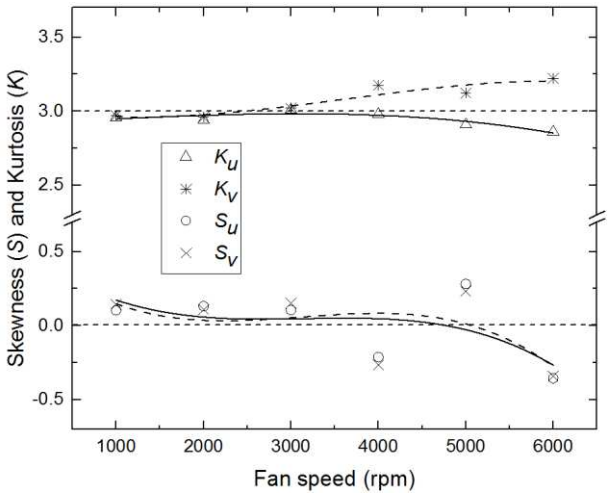

Figure 8. Effect of fan speed on skewness and kurtosis factors.

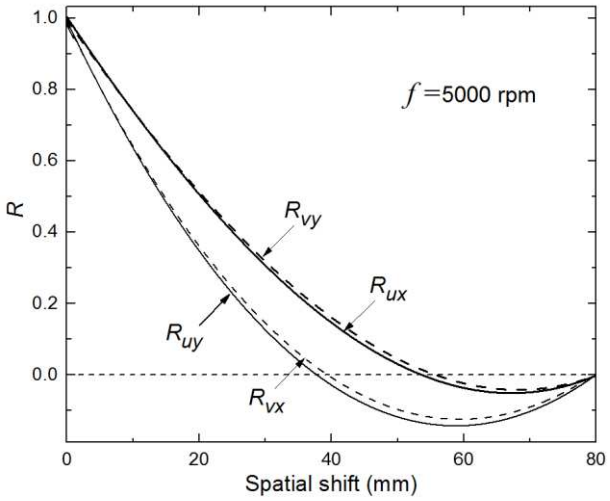

Figure 9. Spatial correlation curves of R_{ux}, R_{vy}, R_{uy} and R_{vx}, for a fan speed of 5,000 rpm.

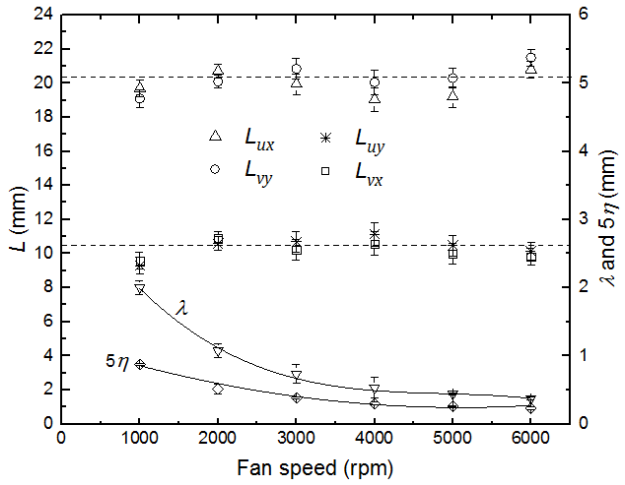

Figure 10.Variations of length scales with fan speed.

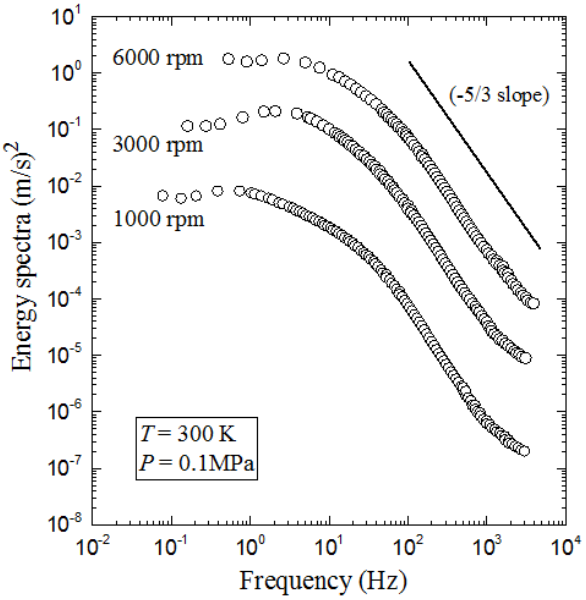

Figure 11. Experimental energy spectra at three fan speeds 1,000, 3,000 and 6,000 rpm.

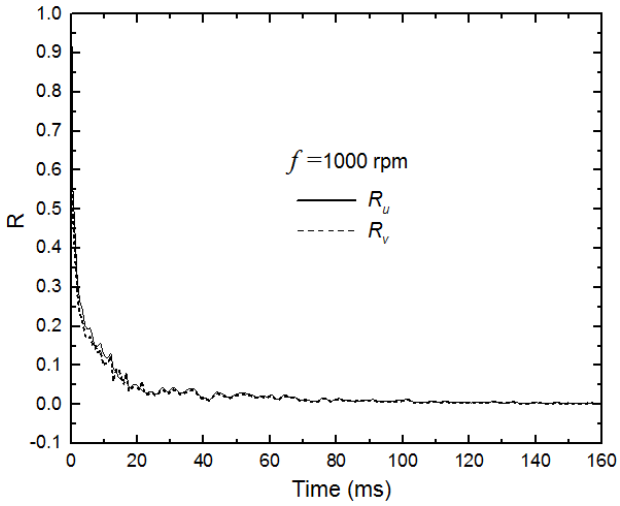

Figure 12.Temporal correlation curves R_u and R_v for fan sped 1,000 rpm.

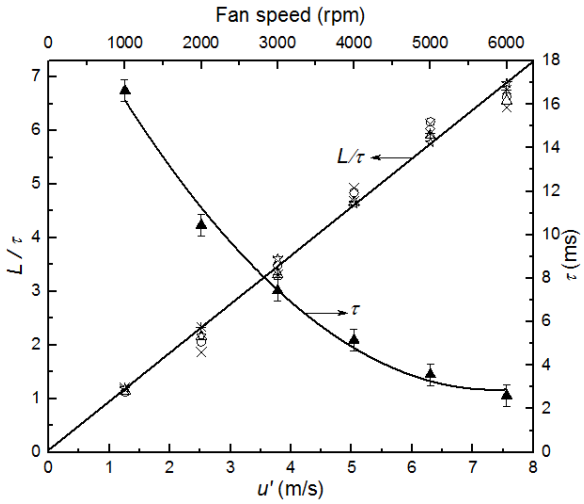

Figure 13. Ratio of turbulence integral length scale to integral time scale, L/τ, versus u'.

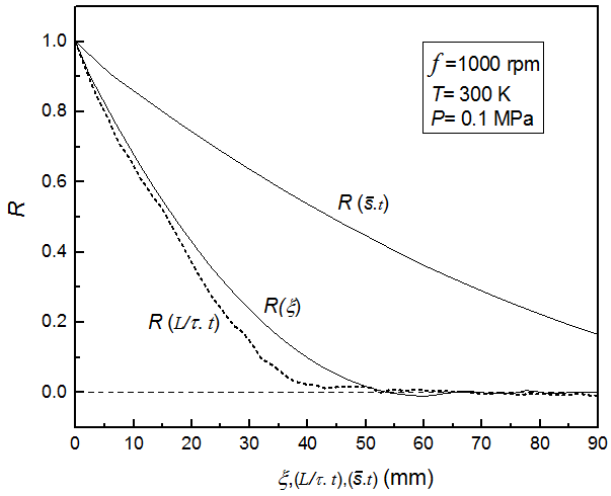

Figure 14. Mean temporal and longitudinal correlation curves for a fan speed of 1000 rpm.

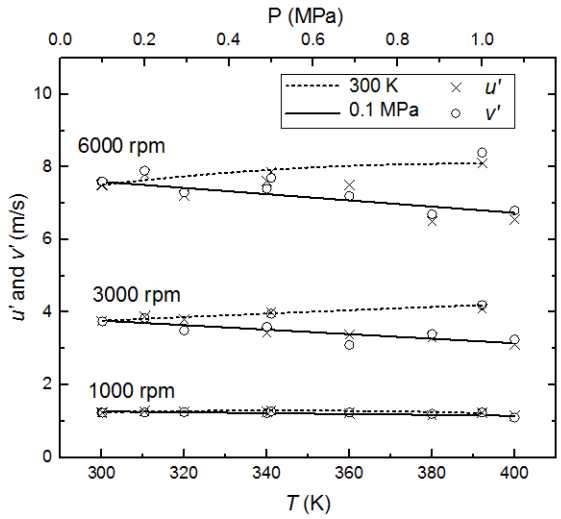

Figure 15. Shows, by solid curves, the effect of temperature on u' and v' at 0.1 MPa and, by broken curves, the effect of temperature on u' and v' at 300K.

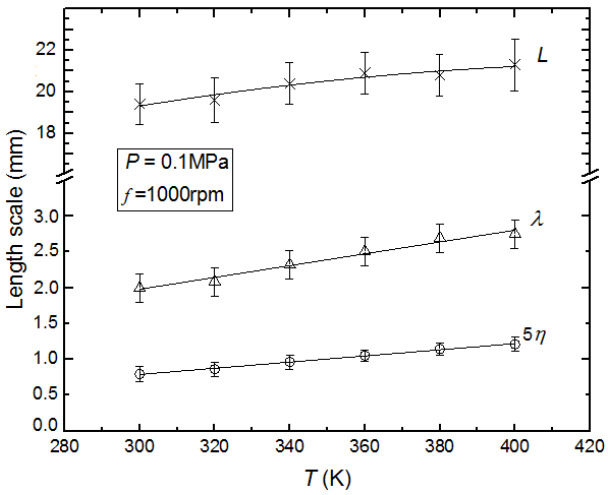

Figure 16. Effect of temperature on length scales at a fan speed of 1,000 rpm.

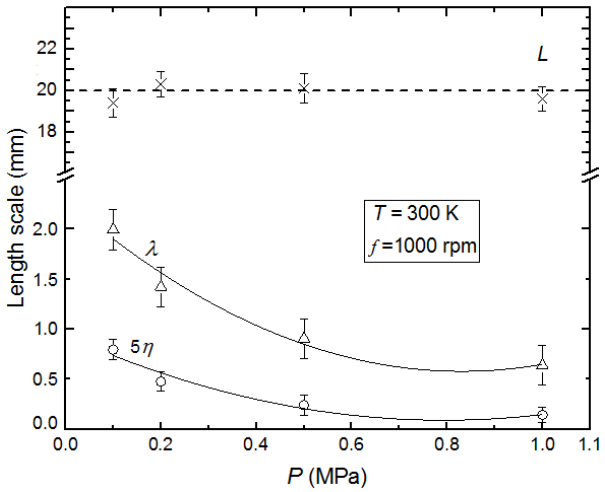

Figure 17. Effect of pressure on length scales at a fan speed of 1,000 rpm.